© 2016. Published by The Company of Biologists Ltd | Journal of Experimental Biology (2016) 219, 2048-2059 doi:10.1242/jeb.132514

RESEARCH ARTICLE

A biorobotic model of the suction-feeding system in largemouth bass: the roles of motor program speed and hyoid kinematics

Christopher P. Kenaley*,‡ and George V. Lauder

ABSTRACT

The vast majority of ray-finned fishes capture prey through suction feeding. The basis of this behavior is the generation of subambient pressure through rapid expansion of a highly kinetic skull. Over the last four decades, results from *in vivo* experiments have elucidated the general relationships between morphological parameters and subambient pressure generation. Until now, however, researchers have been unable to tease apart the discrete contributions of, and complex relationships among, the musculoskeletal elements that support buccal expansion. Fortunately, over the last decade, biorobotic models have gained a foothold in comparative research and show great promise in addressing long-standing questions in vertebrate biomechanics. In this paper, we present BassBot, a biorobotic model of the head of the largemouth bass (*Micropterus salmoides*). BassBot incorporates a 3D acrylic plastic armature of the neurocranium, maxillary apparatus, lower jaw, hyoid, suspensorium and opercular apparatus. Programming of linear motors permits precise reproduction of live kinematic behaviors including hyoid depression and rotation, premaxillary protrusion, and lateral expansion of the suspensoria. BassBot reproduced faithful kinematic and pressure dynamics relative to live bass. We show that motor program speed has a direct relationship to subambient pressure generation. Like vertebrate muscle, the linear motors that powered kinematics were able to produce larger magnitudes of force at slower velocities and, thus, were able to accelerate linkages more quickly and generate larger magnitudes of subambient pressure. In addition, we demonstrate that disrupting the kinematic behavior of the hyoid interferes with the anterior-to-posterior expansion gradient. This resulted in a significant reduction in subambient pressure generation and pressure impulse of 51% and 64%, respectively. These results reveal the promise biorobotic models have for isolating individual parameters and assessing their role in suction feeding.

KEY WORDS: Fish, BassBot, Robotics, Pressure

INTRODUCTION

The majority of ray-finned fishes (actinopterygians) capture prey by suction feeding, a behavior dependent on the generation of subambient pressure through rapid expansion of the buccal cavity (Fig. 1). For nearly half a century, the biomechanical basis of aquatic suction feeding in fishes has attracted the attention of comparative biologists. As a result, there exists a generalized understanding of the functional role played by major musculoskeletal units of the teleost head (for reviews, see Ferry-Graham and Lauder, 2001; Westneat, 2005; Day et al., 2015). Rapid expansion of the buccal cavity results from orchestrated movements of linkages that form a highly kinetic skull, including rotation of the lower jaw, ventral rotation and depression of the hyoid apparatus, lateral expansion of the suspensoria, and dorsal rotation of the cranium about the axial skeleton (Alexander, 1967; Lauder, 1980a, 1985).

This model of suction feeding is based largely on data from *in vivo* experimentation on a number of ray-finned fishes, in addition to more recent work on selected elasmobranchs (e.g. Motta and Wilga, 2000; Nauwelaerts et al., 2008; Wilga and Sanford, 2008). Feeding sequences of live animals have been analyzed for kinematic, pressure and water-flow patterns, as well as other variables linked to suction performance (e.g. Grubich and Wainwright, 1997; Lauder et al., 1986; Sanford and Wainwright, 2002; Day et al., 2007). As a complement to *in vivo* experimentation, a few studies have involved computational models of the teleost suction-feeding system (e.g. Carroll et al., 2004; Drost et al., 1988; Holzman et al., 2012; Osse and Muller, 1980; Van Wassenbergh and Aerts, 2009), and surgical alterations of head morphology have provided further insights into the functional relationships among mechanical linkages (e.g. Lauder, 1980b, 1983; Liem, 1970). As a whole, experimental and modeling approaches have yielded important insights into the mechanistic relationships between morphological parameters and suction performance. Despite this, there remain fundamental questions surrounding several aspects of suction feeding in ray-finned fishes. Because of the complexity of the interactions among the many skeletal and muscular elements of the head, it has proven exceptionally difficult to tease apart the contributions of individual mechanical linkages to suction-feeding performance. In particular, the relationship between the complex motion of musculoskeletal elements in the head and negative pressure generation inside the buccopharyngeal cavity, as well as the discrete contributions to suction generation of each musculoskeletal unit, is still not clear (Sanford and Wainwright, 2002; Wainwright et al., 2007). To address questions such as these and understand the influence of individual components of suction-feeding systems of fishes, it is clear that a new line of attack is required. Studies of feeding systems in live animals are limited in their ability to determine causal relationships between kinematics and suction performance.

Fortunately, a promising avenue of research in vertebrate biomechanics has risen to the fore over the last decade: biorobotic models. Based on abstractions of morphological details and precise motion programs, biorobotic models of vertebrate musculoskeletal systems permit isolation of individual parameters and evaluation of a broad parameter space. The application of biorobotic models has proven particularly illuminating in the study of fish locomotor systems and aquatic propulsion, permitting researchers to evaluate how fishes generate thrust, the manner of hydrodynamic interactions between sets of fins, and how inherent material properties and kinematic programs affect locomotor efficiency (Esposito et al.,

Museum of Comparative Zoology, Harvard University, Cambridge, MA 02138, USA. *Present address: Department of Biology, Boston College, Chestnut Hill, MA 02467, USA.

‡Author for correspondence (kenaley@bc.edu)

C.P.K., 0000-0003-3832-7001

Received 23 September 2015; Accepted 21 April 2016

Journal of Experimental Biology

Journal of Experimental Biology (2016) 219, 2048-2059 doi:10.1242/jeb.132514

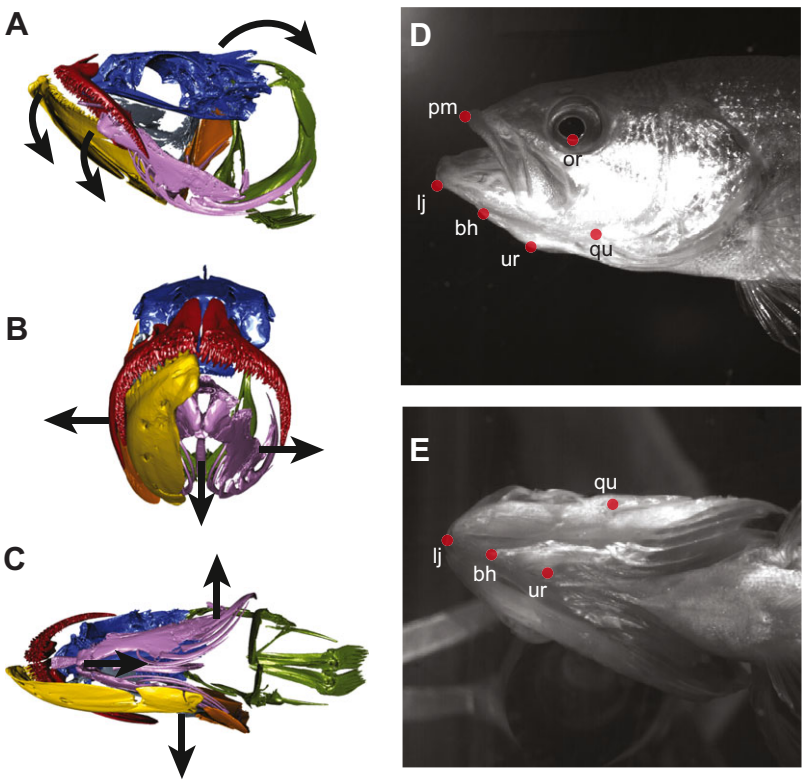

Fig. 1. The species modeled in robot development, the largemouth bass (*Micropterus salmoides*). (A–C) The skeletal units of the cranium with left lower jaw, suspensorium and opercular apparatus removed. Black arrows represent the typical kinematic trajectories during suction feeding. Neurocranium, blue; maxillary apparatus, red; lower jaw, yellow; hyoid apparatus, purple; opercular apparatus, orange; pectoral girdle, green. (A) Left-lateral view, (B) anterior view and (C) ventral view. (D) Lateral and (E) ventral frames captured from high-speed videography of a feeding experiment with landmarks indicated by red dots: anteroventral tip of the lower jaw (lj), anterior-most point of the premaxilla (pm), ventral-most point along the fleshy orbit (or), ventral margin of the quadrate (qu) between the quadrato-articular joint and anteroventral tip of the preopercle, anterior basihyal (bh) and anterior urohyal (ur).

2012; Lauder et al., 2007, 2011). Perhaps as a result of the skeletal and kinematic complexity of the actinopterygian head, no biorobotic models have been developed for any fish feeding system. The development of robotic feeding models will permit scientists to study feeding in novel ways. Comparative studies of feeding in fishes, although likely to continue yielding valuable data, are limited by an inability to control non-feeding variables that differ between species and an inability to isolate any one morphological variable. In addition, *in vivo* experimentation is often confounded by idiosyncratic feeding behavior (e.g. loss of motivation during feeding; Lauder, 1980b).

In this paper, we present the design of 'BassBot', a first-generation biorobotic model of the ray-finned fish suction-feeding system based on the morphology of the largemouth bass (*Micropterus salmoides* Lacépède). BassBot incorporates a 3D armature of the bass head fabricated from acrylic plastic. The hard anatomy of the model represents the functional units of the actinopterygian head including the neurocranium, maxillary apparatus, lower jaw, hyoid, suspensorium and opercular apparatus (Fig. 1). Constrained by the properties and positions of joints found in the bass skull and actuated by motors representing the muscles that power buccal expansion, the 3D kinematic profiles of these units are precisely controlled. Programming of motors permits precise simulation of kinematic behaviors, including hyoid depression and rotation, premaxillary protrusion, and lateral expansion of the suspensoria. The goal of developing this prototype was to fabricate a robotic system that produces behaviors generally similar in kinematics and negative-pressure generation to those of a largemouth bass. We simultaneously set out to demonstrate the promise of biorobotic feeding models by first comparing model behavior and pressure performance with data obtained from *in vivo* feeding experiments in unrestrained bass, and then addressing several longstanding questions in suction feeding through experiments that isolate and alter model parameters. Our specific experimental goals were (1) to evaluate the relationship between the speed of buccal expansion and suction performance, and (2) to assess the contribution of the hyoid apparatus to subambient pressure generation.

MATERIALS AND METHODS

Study species and specimens

Our robotic system was modeled after the largemouth bass, a species readily available in collections and from commercial sources. This facilitated easy acquisition of specimens for morphological characterization and feeding experiments. In addition, this species has been the subject of previous analyses, including the classic paper by Nyberg (1971) and a number of studies that evaluated the functional role of musculoskeletal units in feeding (e.g. Camp and Brainerd, 2014; Camp et al., 2015; Lauder, 1983; Richard and Wainwright, 1995; Wainwright and Richard, 1995) and several that explored the relationship between musculoskeletal morphology, kinematics and suction generation (e.g. Carroll et al., 2004; Grubich and Wainwright, 1997; Higham et al., 2006a,b). Thus, the choice of this species permitted manageable integration of morphological data with kinematic, behavioral and pressure performance data that together informed the design requirements of our robotic model.

Feeding experiments were based on three individuals (14.7, 18.4 and 19.9 cm standard length, SL) purchased from Wiining Aquaculture (Gardner, MA, USA), and kept in individual 40 l aquaria under a 12 h:12 h light:dark cycle. Fish were fed earthworms daily until 2–3 days before feeding experiments. Fish were handled ethically according to Harvard University Institutional Animal Care and Use Committee guidelines, protocol 20-03.

Morphological data for model design came from analyses of preserved specimens. A 3D model of the skeletal structure of a single specimen, MCZ (Museum of Comparative Zoology, Harvard University) 48917 (17.8 cm SL), was reconstructed

Journal of Experimental Biology (2016) 219, 2048-2059 doi:10.1242/jeb.132514

from micro-computed tomography (μCT) analysis (Fig. 1A–C). Scan parameter values for amperage, voltage, exposure time and image rotation were 60 μA, 130 kV, 625 ms and 0.5 deg, respectively. The scan produced images with a voxel size of 38 μm. After slice reconstruction in NRecon (Micro Photonics, Inc., Allentown, PA, USA), volume was rendered in Mimics 15.0 (Materialise, Leuven, Belgium). Additional skeletal data were obtained from a 21.2 cm skeletonized specimen (MCZ 154227). Muscle geometry, including positions of origin and insertion, was recorded from dissections of four specimens (MCZ 48917, 15.3–19.4 cm SL).

Feeding kinematics

The motions of musculoskeletal units of the bass feeding system were studied by filming each of three individuals with two Photron Fastcam PCI-2014 cameras (resolution: 1024×1024 pixels; Photron, San Francisco, CA, USA) in lateral and ventral views. Both cameras filmed at a rate of 1000 frames s^{-1} and were digitally synchronized. Each bass was fed five times over the course of a single series of trials in a 28×28×80 cm (width×depth×length) tank for a total of 15 trials. Feedings were initiated at approximately 10 min intervals by dropping a small (1.5 cm) piece of earthworm through a tube 2.5 cm in diameter.

For each trial, six points on the bass head were digitized in lateral and ventral views (Fig. 1D–E): anteroventral tip of the lower jaw (1), anterior-most point of the premaxilla (2), ventral-most point along the fleshy orbit (3), ventral margin of the quadrate between the quadrato-articular joint and anteroventral tip of the preopercle (4), anterior basihyal (5) and anterior urohyal (6). These points were digitally calibrated with Hedrick's (2008) custom-written MatLab program (The Mathworks, Natick, MA, USA) to produce 3D representations of their position in ventral and lateral views. From these data, we calculated the following kinematic variables as 3D Euclidean distances: gape (premaxilla to tip of lower jaw); premaxillary protrusion (eye to tip of premaxilla); anterior hyoid depression (basihyal to eye); and posterior hyoid depression (urohyal to eye). Suspensorial expansion was calculated as the minimum normal distance between the anguloarticular joint and a plane defined by the basihyal, urohyal and lower jaw. Calculations of kinematic variables were undertaken in R (http://www.R-project.org/).

Robotic design and performance objectives

The design and behavioral objectives for BassBot were based upon our *in vivo* feeding experiments and the results of previous studies investigating the feeding kinematics and suction performance of the largemouth bass (e.g. Camp and Brainerd, 2014; Carroll et al., 2004; Grubich and Wainwright, 1997; Higham et al., 2006a,b). In particular, we set out to design a prototype that (1) comprised the major musculoskeletal units involved in suction feeding, (2) produced kinematic profiles similar to live bass, and (3) generated pressure profiles similar in magnitude and shape to those recorded in these previous *in vivo* studies. We required that BassBot include the following structural elements: neurocranium, lower jaw, maxilla and premaxilla, hyoid apparatus and suspensorium. Motion profile objectives included lower jaw rotation about the quadrate of the suspensorium, premaxillary protrusion powered by rotation of the lower jaw, hyoid rotation and retraction, and suspensorial abduction driven by retraction of the hyoid and lateral rotation of the hyoid bars. Actuation was implemented with individually programmable linear motors attached to cables that mimic lines of action of the muscles involved in suction: the adductor mandibulae, levator operculi, sternohyoideus and axial muscles.

Robot experimentation

Two sets of experiments were undertaken with BassBot: for experiment I, we assessed the effect of motor-program speed on kinematic behavior and pressure performance, while in experiment II we assessed the contribution of hyoid kinematics to subambient pressure generation. In experiment I, we compared kinematic variables and subambient pressure within the buccal cavity in a set of control trials (N=5) with those for a set of trials in which the time to peak linear-motor displacement was increased by 25% ('slow', N=5; Fig. 2). The relative timing of individual motor programs that control the kinematic profiles of the robotic functional units was based upon the results of our *in vivo* feeding experiments. Because of performance limitations of the linear motors, the absolute timing of control trials could not be reproduced with similar absolute values to live bass in terms of mouth opening speed. Thus, our experimental focus in these initial trials was to evaluate the effect of kinematic speed on negative pressure generation under relative kinematic timing patterns similar to a live bass.

In experiment II, we compared negative-pressure generation between a set of control trials (N=5) and a set of trials in which hyoid motion was restricted (N=5). For the control trials of this second experiment, we implemented a motor program with displacements identical to the control of our first experiment; however, time to peak linear-motor displacement was decreased by 50% to permit more forceful motor input. In our second set of trials for this experiment, we restricted movements of the hyoid apparatus by placing a stiff rubber band around the ventral processes of the robotic quadrates. This permitted hyoid depression relative to the neurocranium, but limited hyoid rotation relative to the lower jaw and abduction of the suspensoria through the action of the hyoid bars.

The motion of BassBot was analyzed by filming each feeding simulation at 500 frames s^{-1} with a single Photron camera shooting in lateral view. The ventral view of BassBot was captured by placing a mirror below the model at 45 deg relative to vertical. For each trial, we digitized six points on the robotic system that correspond to the same points analyzed in the *in vivo* experiments (see below). 2D analysis of these points was undertaken with MTrackJ (Meijering et al., 2012), as implemented in ImageJ (http://imagej.nih.gov/ij/). From these data, we calculated the same kinematic variables as for the *in vivo* experiments, with one exception: suspensorial expansion was calculated as the distance between the ventral processes of

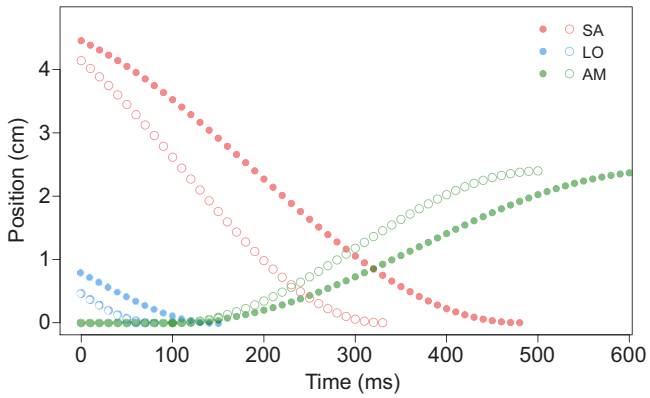

Fig. 2. Plot of displacement versus time for linear motors during biorobotic experiment I. In trials 6–10 (i.e. 'slow' trials), velocity for all three motor programs was increased 25% over control trials 1–5. The linear motors function as the adductor mandibulae complex (AM), sternohyoideus-axial musculature (SA) and levator operculi (LO).

Journal of Experimental Biology (2016) 219, 2048-2059 doi:10.1242/jeb.132514

robotic quadrate bones. We were able to digitize the kinematic variables in 2D (as opposed to 3D in the live bass) because the model was positioned precisely parallel to the camera. We also used the 2D coordinates of the robotic landmarks in each plain from experiment I to estimate the percentage change in volume between open and closed positions of BassBot. The robotic units often undertook excursions of extremely low velocity near peak displacement. To remove this noise, we computed peak displacement by comparing slopes over a sliding window of 10 ms and considered displacement to be at the peak when slope angle exceeded 45 deg.

Suction performance in BassBot was assessed with two catheter-tip pressure transducers (model SPR-S24, Millar Instruments, Houston, TX, USA) that were passed through cannulae placed through the neurocranium: one in the anterior and one in the posterior region of the buccal cavity (Fig. 3A). Pressure data were digitized at a rate of 1000 Hz through a Powerlab 8SP data acquisition system (ADInstruments, Colorado Springs, CO, USA), passed to LabChart (ADInstruments) and synchronized with a 3 V signal from the motor controllers. High-frequency noise in the pressure data was removed with a 10 Hz low-pass filter in LabChart. From these pressure data, we calculated the time to peak subambient pressure, the magnitude of peak subambient pressure, and impulse. Impulse was calculated as the area within the subambient pressure trace and represents an estimation of the energy imparted to water by robotic movement (see Lauder and Shaffer, 1985; Lauder et al., 1986). Variable means for each treatment within experiments I and II were compared with a two-sample Student's *t*-test.

RESULTS

Robot design and fabrication

Our initial goal of fabricating a biomimetic robotic model of the largemouth bass was realized in our BassBot prototype. BassBot (Fig. 3) consists of a skeletal armature cut from polymethyl methacrylate (PMMA) transparent thermoplastic using a Zing 16 40 W laser cutter (Epilog, Golden, CO, USA). Shapes of each functional unit were informed by data taken from skeletonized and dissected specimens in addition to the μCT 3D models. The lower jaw consists of two symmetrical pieces of PMMA articulating at an anterior symphysis via a pinless polypropylene hinge (Super Flex Poly Hinge, Super-Tronics, Elkins Park, PA, USA; Fig. 1B). To permit off-axis rotation and suspensorial abduction/adduction, the lower jaw articulates to the ventromedial tip of the suspensorium via an aluminium ball joint (model S592, Sullivan Products, Baltimore, MD, USA; Fig. 1E). The suspensorium articulates with the neurocranium via two Super Flex pinless hinges along a

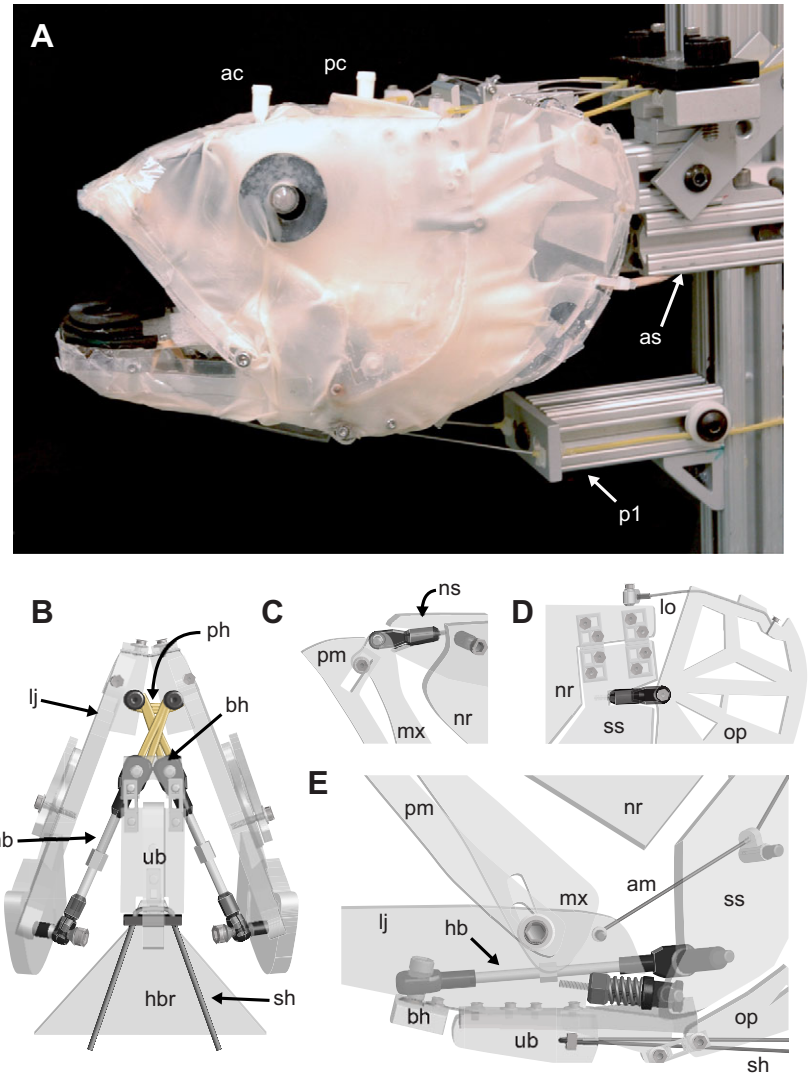

Fig. 3. Biorobotic model of the suction-feeding system of the largemouth bass (*M. salmoides*). (A) Lateral view of the robotic cranium mounted to an aluminium axial skeleton (as) and pectoral girdle (p1) with biomimetic skin covering hard skeletal elements cut from PMMA thermoplastic. Anterior and posterior canulae (ac and pc, respectively) pass into the oral cavity and accept two catheter-tipped pressure transducers. (B) Ventral view of the lower jaw (lj) and hyoid and branchial apparatus, including hyoid bars (hb); basihyal (bh), urohyal-basibranchial unit (ub) and hypobranchial (hbr); a Teflon-coated wire tendon passes through the posterior urohyal and is attached to a pair of linear motors representing the sternohyoideus-hypaxial muscle complex (sh). The protractor hyoideus (ph) is represented by a latex band anchored to the lower jaw near the mandibular symphysis and to the anterior hyoid bars. (C) Lateral view of the dorsal maxillary apparatus composed of the premaxilla (pm) and maxilla (mx) pivoting about the robotic nasal bone (ns) via a ball joint. (D) Lateral view of the robotic posterolateral neurocranium (nr) about which the dorsal suspensorium (ss) abducts; the dorsal opercular apparatus (op) articulates with the suspensorium at a ball joint, permitting rotation in the sagittal plane driven by a motor and wire–tendon unit representing the levator operculi (lo). (E) Lateral view of the mandibular-maxillary articulation, quadrato-articular joint, ventral opercular apparatus and hyoid apparatus. A wire–tendon unit inserting along the posteromedial face of the lower jaw and originating at a linear motor represents the adductor mandibulae (am) muscles that adduct the lower jaw.

Journal of Experimental Biology (2016) 219, 2048-2059 doi:10.1242/jeb.132514

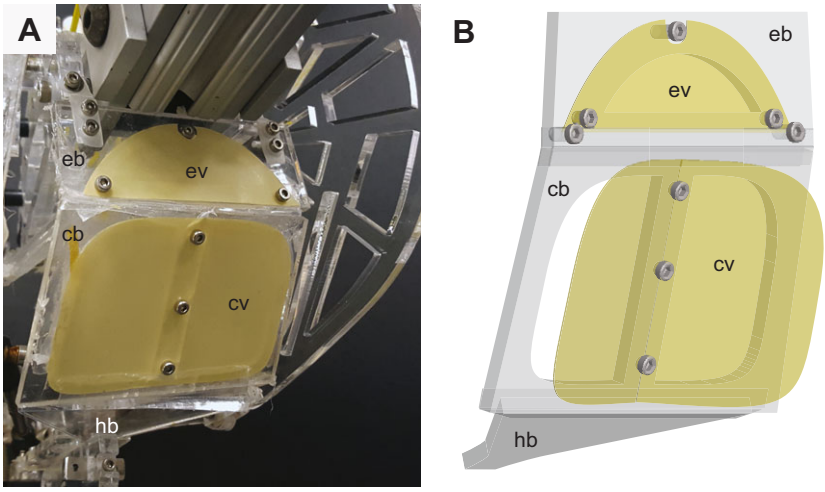

Fig. 4. Schematic representation of the branchial apparatus of a biorobotic model of the suction-feeding system of the largemouth bass (*M. salmoides*). Posterior view (A) and schematic diagram (B) of the PMMA thermoplastic hypobranchial (hb), ceratobranchial (cb) and epibranchial (eb) units. The open areas in the ceratobranchial (cb) and epibranchial (eb) units are covered on their posterior faces by a ceratobranchial (cv) and epibranchial valve (ev), respectively.

dorsoposterior flange meant to represent the articulating surfaces of the pterotic and sphenotic bones (Fig. 3D). The maxilla articulates with the lower jaw via a socket-head bolt (Fig. 3B,E) and with the neurocranium via a swivel-ball joint representing the articulating surface of the nasal (Fig. 3C), thus permitting anterior–posterior rotation and lateral abduction. Motion along the mandibular-maxillary articulation is constrained by a bolt in a C-shaped groove within the ventral heads of the maxilla and premaxilla (Fig. 3E). The hyoid apparatus rotates ventrally about 12.7 mm low-density polyethylene (LDPE) spacers that represent the interhyals (Fig. 3B,E). The LDPE interhyals are fixed to the suspensorium by a bolt and articulate with a ball joint of a 59 mm turnbuckle (model RVXL/SLH, Traxxas, Plano, TX, USA) that represents the bones of the hyoid bar (i.e. epihyal, ceratohyal and hypohyal). At their anterior ends, the ball joints of the two hyoid bars articulate with a PMMA basihyal (Fig. 3B,E). In addition to permitting ventral rotation, ball joints at either end of the hyoid bar turnbuckle permit lateral abduction of the posterior head of the bars and, through their fixed interhyal linkages, lateral abduction of the suspensoria. The entire robotic head is fixed to an aluminium spine (Fig. 3A).

The basihyal articulates with a PMMA urohyal-basibranchial unit via two halves of a Super Flex hinge (Fig. 3B). The urohyal-basibranchial unit articulates with a triangular unit representing the hypobranchials of the gill arches via one half of a Super Flex hinge (Fig. 3B,C). The PMMA hypobranchial unit articulates with a square-shaped PMMA ceratobranchial unit, in which are cut two open hemispheres (Fig. 4). This ceratobranchial unit articulates with a PMMA epibranchial that has a single hemisphere cut within it (Fig. 4). Both the hypobranchial-ceratobranchial and ceratobranchial-epibranchial articulations are secured with waterproof Fix-It Tape (Top Tape & Label, Wheatfield, NY, USA). Each open hemisphere is covered on its posterior face with a valve cut from 0.102 mm tan polyester shim stock, thus restricting the posterior to anterior flow of water into the buccal cavity during

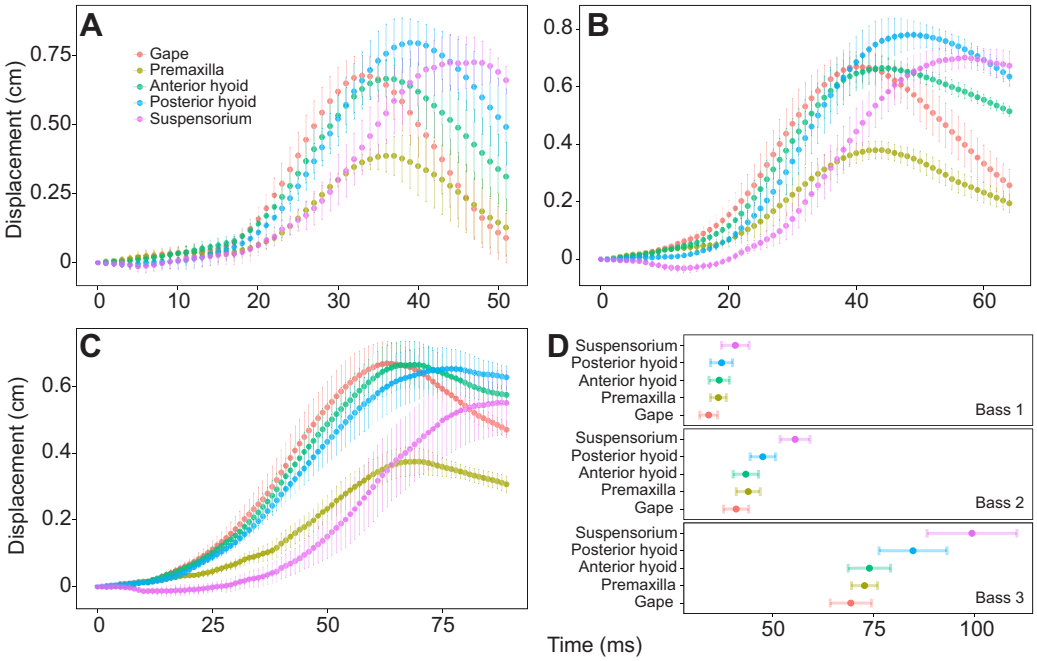

Fig. 5. Plots of kinematic variables during feeding in live largemouth bass. (A–C) Kinematic profiles of buccal expansion during feeding in each of the three bass specimens studied (bass 1–3, respectively). (D) Bar plot of time to peak displacement for each kinematic variable for each of the three bass specimens. *N*=5 feeding events. Data points and whiskers in plots represent the mean±1 s.e.m.

Journal of Experimental Biology

Journal of Experimental Biology (2016) 219, 2048-2059 doi:10.1242/jeb.132514

Table 1. Pressure variable comparison for robotic experiment I in which time to peak motor excursion was increased 25%

	Time to peak (ms)		Peak pressure (Pa)		Impulse (N s)	
	Anterior	Posterior	Anterior	Posterior	Anterior	Posterior
Control	95.8±4.4	101.8±5.1	−442.9±4.5	−405.9±31.5	44.1±26.1	44.1±6.2
Slow	87.8±0.6	95.4±0.4	−639.2±1.2	−618.7±15.5	63.0±22.0	86.3±1.9
Change	−80.0	−6.4	−196.3	−212.8	18.9	42.2
t	1.82	1.25	5.59	6.24	4.07	6.53
P	0.14	0.279	0.002	<0.001	0.012	0.002

Data for control and slow trials are means±s.e.m. Variable means were compared with a two-sample Student's *t*-test.

expansion (Fig. 4). The epibranchial unit is fixed to the posterior face of a hemispherical tube that forms the roof of the buccal cavity (Fig. 3). This effectively isolates the buccal cavity and follows Lauder (1983), who found that pressure changes in the opercular cavity did not alter pressure in the buccal cavity during suction feeding. Furthermore, because the buccal cavity is isolated and its hydrodynamics are independent of an opercular cavity, we did not include a functional opercular chamber in our model.

Five Quickshaft linear DC servomotors (model LM 2070-80-1, Faulhaber, Schönaich, Germany) are integrated as the muscular actuation. Two linear motors function as the adductor mandibulae complex (AM), two as the sternohyoideus-hypaxial musculature (SA) and one as the levator operculi (LO). Motors are affixed to their insertion points via tendons consisting of 0.5 mm diameter Teflon-coated stainless-steel wire passed through flexible cable housing. Tendon geometry is based on data recorded from dissections of preserved specimens and µCT analysis. The AM motor tendons pass through a nylon control-horn bracket (model DUB559, Du Bro RC, Wauconda, IL, USA) on the medial faces of the PMMA suspensoria and insert on the medial face of the mandible. The LO motor tendons emerge from control-horn brackets on the posterodorsal aspect of the PMMA neurocranium and insert on to the dorsal edge of the PMMA opercular unit. The SAM motor tendons originate from an aluminium pectoral girdle (Fig. 3A) and insert on the ventral aspect of the urohyal (Fig. 2B). Speed and position of each mechanical unit is programmable with a customized Advanced Serial Write and Read virtual instrument in LabView (National Instruments, Austin, TX, USA).

The entire head of the robotic model is enveloped in ultrathin, 150 µm thick, natural rubber latex to represent the skin (Fig. 3A). This skin analog is attached in two symmetrical pieces to the PMMA skeleton by waterproof Fix-It Tape. These two contralateral pieces are joined at a seam oriented along the ventral midline of the robotic jaw and hyoid apparatus, and adhere posteriorly to the lateral

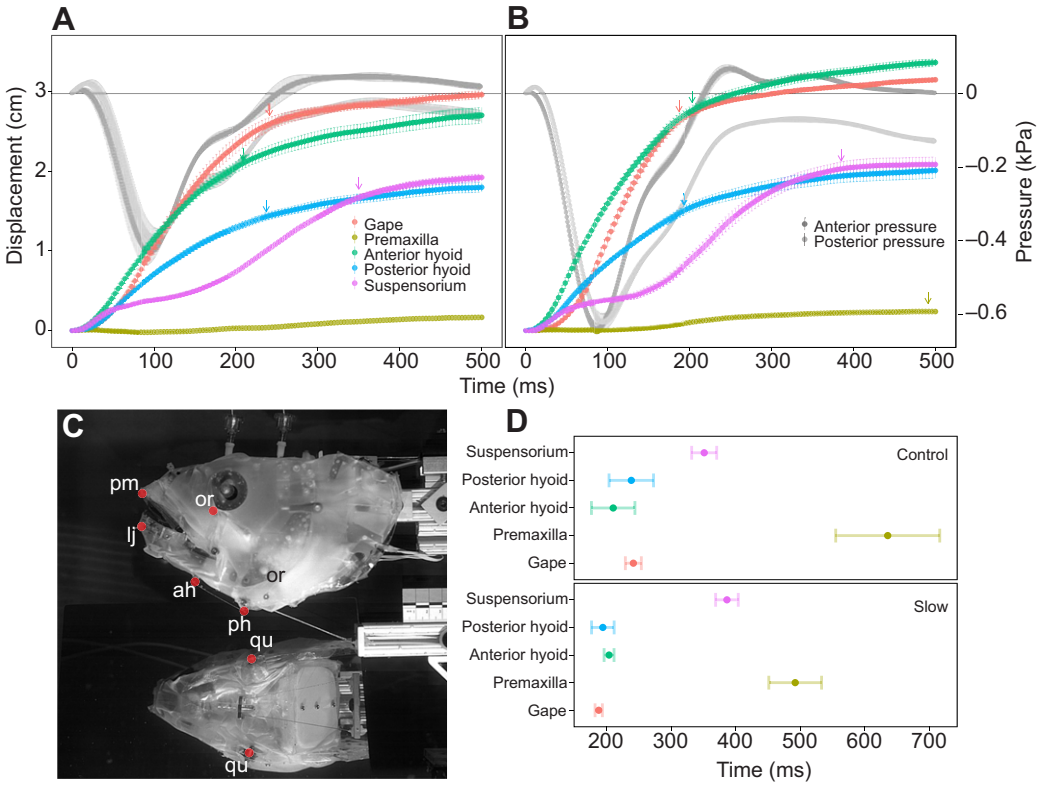

Fig. 6. Plots of robotic kinematic variables during experiment I. (A) Kinematic and pressure profiles of robotic buccal expansion during 'control' trials (*N*=5). (B) Kinematic and pressure profiles of robotic buccal expansion for trials in which the velocity of the three linear motor units was decreased 25% relative to control trials (i.e. 'slow' trials, *N*=5). (C) BassBot model showing the position of points recorded for kinematic variables: anteroventral tip of the lower jaw (lj), anterior-most point of the premaxilla (pm), ventral orbit (or), ventral margin of the robotic quadrate (qu), anterior hyoid (ah) and posterior hyoid (ph). (D) Bar plot of time to peak displacement for each robotic kinematic variable for control and slow experiments. Data points and whiskers in A, B and D represent the mean±1 s.e.m. Arrows in A and B correspond to peak displacement as described in Materials and methods.

Journal of Experimental Biology (2016) 219, 2048-2059 doi:10.1242/jeb.132514

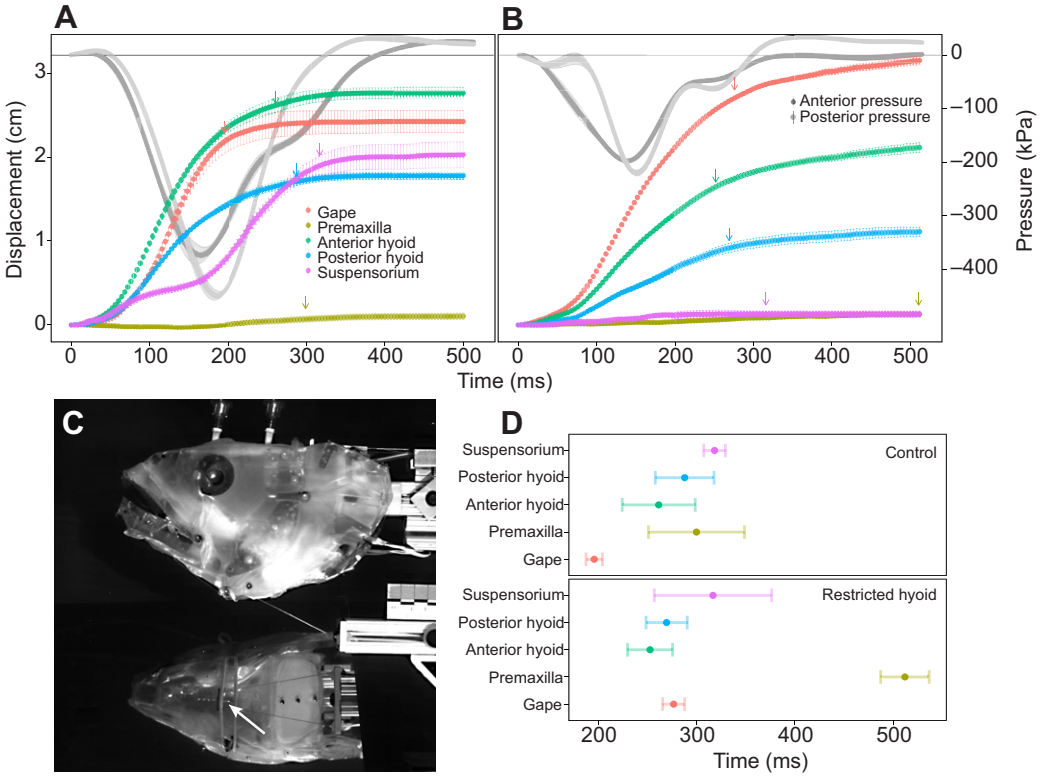

Fig. 7. Plots of robotic kinematic variables during experiment II. (A) Kinematic and pressure profiles of robotic buccal expansion during control trials (*N*=5). (B) Kinematic and pressure profiles of robotic buccal expansion for trials in which the hyoid was restricted (*N*=5). (C) BassBot model with elastic band (white arrow) attached between robotic quadrates and across the ventral hyoid apparatus, limiting suspensorial abduction and hyoid depression relative to the lower jaw. (D) Bar plot of time to peak displacement for each robotic kinematic variable for control and slow experiments. Data points and whiskers in A, B and D represent the mean±1 s.e.m. Arrows in A and B correspond to peak displacement in D, as described in Materials and methods.

margins of the ceratobranchial and epibranchial units. Dorsally, the latex is taped to the premaxillary symphysis and is joined via Fix-It Tape along the dorsal midline seam. The seam starts within the buccal cavity between the two premaxillae, forming a dorsal oral valve, and continues along the outside of the premaxillary symphysis of the neurocranium. The anterior dorsal tip of the lower jaw was affixed with a 3 mm-thick, U-shaped neoprene strip to represent the ventral oral valve.

In vivo and robotic kinematic behavior

The live bass demonstrated consistent patterns of kinematic activity (Fig. 5A–C): gape, premaxillary and anterior hyoid displacement began nearly simultaneously, followed by the posterior hyoid after approximately 15 ms and then suspensorial expansion after approximately 20 ms (Fig. 5C). In all three bass, the gape, premaxilla and anterior hyoid reached peak displacement in close succession (Fig. 5A–C). This was followed by peak posterior hyoid displacement and then by peak suspensorial abduction. Gape, anterior and posterior hyoid, and suspensorial displacements reached similar magnitudes. In bass 1 and 2, the posterior hyoid achieved the largest mean magnitude of displacement, followed by suspensorial abduction, then gape and anterior hyoid, variables that attained nearly identical excursion distances. In bass 3, mean gape and anterior and posterior hyoid displacements were nearly identical, while mean suspensorial displacement was much less. In all three specimens, the premaxilla attained magnitudes of mean displacement equal to approximately half of the gape and hyoid displacements (Fig. 5A–C).

Similarly, BassBot demonstrated consistent kinematic patterns for each experimental treatment (Figs 6 and 7). Gape and anterior hyoid reached similar magnitudes of displacement, as did the posterior hyoid and suspensorial displacement. Under all experimental conditions, premaxillary displacement was minimal. Displacement of the robotic suspensorium and posterior hyoid reached approximately half the displacement of the gape and anterior hyoid in experiments where the hyoid was unrestrained (Figs 6A,B and 7A). Robotic gape and anterior and posterior hyoid reached peak displacement in close succession followed by peak suspensorial abduction (Fig. 6A,B,D). Kinematic displacement resulted in mean buccal cavity volume change of 77% for all trials in experiment I (Fig. S1).

Robotic experiment I: effect of motor program speed

In this experiment, we compared the effect of increasing the time to peak linear-motor excursion by 25% over the control (Fig. 2) on robotic kinematic behavior and subambient pressure generation. In terms of kinematic behavior, this ‘slow’ treatment, which was designed to prolong the feeding event, had the unexpected effect of increasing peak kinematic displacement for all measured variables and reducing the time to peak kinematic displacement for all variables except suspensorial abduction (Fig. 6D). Peak displacements of the premaxilla, anterior hyoid and suspensorium were significantly greater in slow trials versus control (P=0.014, 0.013 and 0.017, respectively). In terms of time to peak displacement, slower motor programs only resulted in a significant reduction for gape (P=0.009). However, there was no significant difference in the estimated relative change of buccal cavity volume between these two treatments (Fig. S1; P=0.41, t=0.86).

Slower motor program speed also unexpectedly increased the magnitude of peak subambient pressure and pressure impulse

Journal of Experimental Biology (2016) 219, 2048-2059 doi:10.1242/jeb.132514

Table 2. Pressure variable comparison for robotic experiment II in which movement of the hyoid apparatus was restricted

	Time to peak (ms)		Peak pressure (Pa)		Impulse (N s)	
	Anterior	Posterior	Anterior	Posterior	Anterior	Posterior
Control	163.8±5.5	181.4±3.3	−380.9±1.8	−453.3±14.5	59.9±9.6	55.7±0.8
Restricted hyoid	134.2±1.2	145.6±1	−198.3±1.3	−221.2±3.7	25.9±5.6	19.9±0.6
Change	−29.6	−35.8	182.5	232.2	−34.0	−35.8
t	5.22	10.24	−12.22	−20.99	−15.52	−35.1
P	0.005	<0.001	<0.001	<0.001	<0.001	<0.001

Data for control and slow trials are means±s.e.m. Variable means were compared with a two-sample Student's *t*-test.

(Figs 6A,B, 8). Time to peak subambient pressure did not change significantly in both the anterior and posterior buccal cavity (P=0.14 and 0.279; Table 1). With slower motor speed, anterior and posterior magnitudes of peak subambient pressure increased significantly (P =0.002 and <0.001, respectively; Table 1). A 25% increase in time to peak motor excursion resulted in a significant increase in anterior and posterior impulse.

Robotic experiment II: effect of restrained hyoid apparatus

In experiment II, we compared the effect of restricting hyoid movement on kinematic behavior and subambient pressure generation. Under these conditions, hyoid retraction was permitted; however, hyoid rotation relative to the lower jaw and lateral expansion and abduction of the suspensoria were limited. As intended, restriction of the hyoid significantly limited peak displacement of the anterior and posterior hyoid and abduction of the suspensoria (all P<0.001). Peak displacement of the anterior and posterior hyoid was reduced by 0.94 cm (37%) and 0.77 cm (46%), respectively, while peak displacement of the suspensoria was reduced by 1.78 cm (93%). In contrast, restriction of the hyoid increased the peak displacement of the gape 0.52 cm (24%) and premaxilla 0.04 cm (44%); however, only the change in gape was significant (P=0.026). Time to peak displacement was unchanged for the anterior and posterior hyoid and suspensorium (P=0.846,

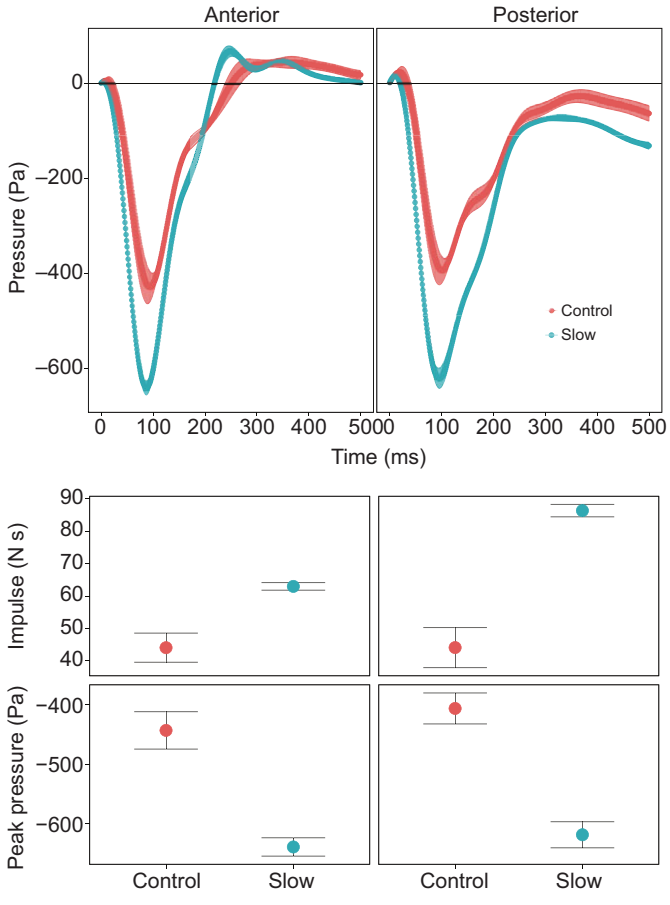

Fig. 8. Negative pressure-generation performance resulting from changes in linear motor program speed during suction feeding. In trials 6–10 (slow), velocity for all three motor programs was decreased by 25% relative to trials 1–5 (control). Solid circles in the upper panel represent mean values; ±1 s.e.m. is shown in a lighter color for each curve. Solid circles in the lower panel represent the change in mean peak subambient pressure and impulse between the control and slow experiments (±1 s.e.m.).

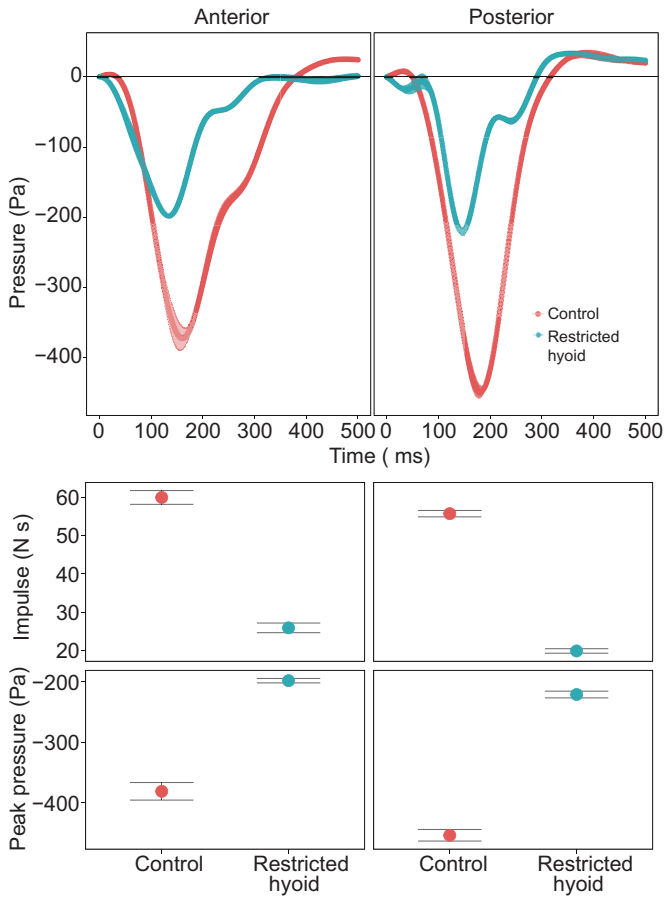

Fig. 9. The effect of restricted hyoid movement on robotic negative pressure generation performance during suction feeding. Solid circles in the upper panel represent the represent mean values; ±1 s.e.m. is shown in a lighter color for each curve. Solid circles in the lower panel represent the change in mean peak subambient pressure and impulse when movement of the robotic hyoid was restricted (±1 s.e.m.).

0.629 and 0.980, respectively). Time to peak gape and premaxillary displacement increased significantly (P=0.001 and 0.008, respectively).

As expected, hyoid restriction resulted in reduced pressure performance as measured by time to peak subambient pressure, magnitude of subambient pressure, and pressure impulse (Table 2, Fig. 9). Time to peak subambient pressure decreased significantly in both the anterior and posterior buccal cavity (P =0.005 and <0.001, respectively; Table 2). Restricting the hyoid also had the effect of decreasing the magnitude of anterior and posterior subambient pressure (both P<0.001; Table 2). In terms of impulse, a restricted hyoid resulted in a significant decrease (both P<0.001; Table 2).

DISCUSSION

In vivo versus robotic feeding behavior

Our robotic system produced biologically faithful kinematic and subambient pressure generation behaviors. Robotic kinematic behavior was similar to live bass behavior and generalized kinematic patterns of suction feeding fishes in that the buccal cavity expansion proceeds in an anterior-to-posterior progression, expanding dorsoventrally and laterally to generate subambient pressure. Dorsoventral expansion in live and robotic bass was accomplished by ventral rotations of the lower jaw and hyoid relative to the neurocranium. After the onset of lower jaw depression, ventral rotation of the hyoid occurred about the articulations of the hyoid bars with the suspensoria. These kinematic patterns resulted in consistent dorsoventral expansion of the floor of the mouth and represent stereotypical behaviors of suction-feeding teleosts in general and of largemouth bass in particular (Richard and Wainwright, 1995).

The buccal cavity of BassBot was laterally expanded via abduction of the suspensoria. As with live suction-feeding teleosts, the force responsible for abduction of the robotic suspensoria resulted from retraction of the hyoid by caudal movement of its posterior linkages. Shortening of our biomimetic ventral muscular element – the sternohyoideus-hypaxial muscle–tendon unit – resulted in the robotic hyoid bars rotating laterally about the anterior of the hyoid apparatus and force transmission to the medial faces of the suspensoria. The lateral expression of the suspensoria from hyoid movement is an established component in suction-feeding fishes (Aerts, 1991; De Visser and Barel, 1996). In addition, the axial muscle–tendon unit was the largest input of force in our robotic system, a characteristic of the system that mirrors recent studies highlighting the great importance of the axial musculature in driving kinematic behavior in suction feeding (Camp and Brainerd, 2014; Camp et al., 2015). The effective transmission of lateral forces to the suspensoria resulting from retraction of linkages posterior to the hyoid also corroborates the hypothesis of other authors (e.g. Aerts, 1991; Day et al., 2015; De Visser and Barel, 1996) that the small levator arcus palatini muscle plays a relatively minor role in suspensorial abduction. Our robotic model did not include this component, yet considerable lateral expansion was achieved.

We also note that we did not include an epaxial muscle unit, but rather only a single axial motor unit that mimicked the hypaxial muscles. The expaxial musculature is an important input that powers rapid expansion in suction feeders (Carroll et al., 2004; Camp and Brainerd, 2014; Camp et al., 2014). However, we argue that, especially for hyoid kinematics, the role of the epaxials is identical to the role of the hypaxials in that shortening by both results in displacement of the hyoid relative to the neurocranium. Thus, expaxial and hypaxial input should result in similar kinematic behaviors of the hyoid and suspensorium. Therefore, the drawback of not including separate expaxial and hypaxial motors is unlikely to be unfaithful kinematic behavior, but rather the inability to assess the discrete effect of each unit separate from the other.

Relative magnitudes of peak excursions in BassBot deviated slightly from our results with live bass and those previously reported. We and Sanford and Wainwright (2002) recorded a similar pattern in live bass in which gape, anterior and posterior hyoid, and suspensorium reach similar peak displacements (Figs 6A,B and 7A). Under control conditions in both experiments I and II, the robotic posterior hyoid and suspensorium reached similar peak displacements that were approximately 60% of peak gape and anterior hyoid excursion. In addition, BassBot was only able to achieve very modest upper-jaw protrusion (Figs 6A,B and 7B). This difference in peak excursion resulted in a reduced volume change of 77%, much less than a live bass (Camp et al., 2015). We suspect that this difference in the pattern of relative excursions is likely due to the limited mimetic properties of our skin analog. The elasticity of the ultrathin latex is invariable across its surface. Thus, linkages with low leverage like the posterior hyoid and suspensoria are more restricted by the robotic skin than the anterior hyoid, which has much greater mechanical advantage.

Premaxillary protrusion is an important behavior in suction-feeding teleosts (Westneat, 2005), acting in part to create an anterior–posterior gradient in buccal cavity volume (Alexander, 1967; Muller and Osse, 1984; Westneat, 2005) and a smaller oral opening that increases water velocity during suction (Lauder, 1980a). The relatively small amount of premaxillary protrusion in the robotic model may also be the result of the relatively stiff latex skin analog. In addition, non-faithful articulations in our robotic model that do not permit proper movements of the linkages may have contributed to the reduced motion. Our design implements a 4-bar linkage represented by the bones of the mandible, suspensorium, nasal and maxillary units that transmits motion of lower jaw rotation to sliding of the premaxilla over the nasal articulation. The articulation of the maxillary and mandibular linkages is not rigid in the largemouth bass as it has been treated in the 4-bar model of other fishes (Westneat, 2004). Our rigid articulation may have hindered premaxillary protrusion by enforcing a limited range of motion for the ventral maxilla. We note again that we did not include an epaxial motor in BassBot. The epaxial muscles are an important component in driving premaxillary protrusion (Liem, 1970, 1978), and thus addition of a mechanical system that modulates head elevation will be a key improvement in future versions of the robotic feeding system.

The relative timing of kinematic events of BassBot during control experiments was similar to those of the live bass and data reported for largemouth bass in the literature (Figs 5D, 6D and 7D; Richard and Wainwright, 1995; Sanford and Wainwright, 2002). The relative timing of peak kinematic positions in our live experiments was nearly identical to previous studies with peak gape, anterior hyoid, posterior hyoid and suspensorial excursions reaching peak magnitudes in that order (Richard and Wainwright, 1995; Sanford and Wainwright, 2002). Our robotic model achieved a slightly different pattern in the two experiments as a result of the implementation of a different motor program. In experiment II, we increased the time to peak excursion for each motor by 50%. Unexpectedly, this did not result in slower times to peak displacement (Tables 1 and 2). As discussed below, the motors that serve as biomimetic muscles are restrained by a force–velocity relationship with decreasing force as velocity increases

Journal of Experimental Biology

Journal of Experimental Biology (2016) 219, 2048-2059 doi:10.1242/jeb.132514

(QuickShaft technical specification sheet, Faulhaber). In the control trials of experiment II, the relative timing of BassBot's peak kinematic variables was nearly identical to patterns reported for largemouth bass (Sanford and Wainwright, 2002), thus demonstrating that our biorobtic system achieved faithful kinematic behavior despite differences in size between our BassBot and live fish.

Because of a faithful reproduction in the timing of expansion kinematics, resulting in an anterior to posterior expansion gradient, the pattern of subambient pressure generation was biologically faithful as well. Peak subambient pressure occurred soon after the initiation of expansion in both the anterior and posterior buccal cavity (Fig. 6A,B), just as in other studies reporting buccal cavity pressure in largemouth bass (Sanford and Wainwright, 2002). In all experiments, anterior subambient pressure peaked before posterior pressure (Figs 8 and 9), a result that indicates biologically mimetic anterior-to-posterior flow of water.

The magnitude of robotic peak subambient pressure generation of 0.35–0.65 kPa (Figs 8 and 9) was much less than published data for live bass of 1–20 kPa (Carroll and Wainwright, 2006; Sanford and Wainwright, 2002). This difference can be attributed to a few factors. First, BassBot undergoes smaller magnitudes of relative volume change. In experiment I, the mean buccal volume increase was 77% (Fig. S1). This represents approximately one-third the volume increase of a live bass (Camp et al., 2015). Second, the kinematic velocities of BassBot were slower than those of live bass. A slower rate of expansion results in lower velocities and accelerations of flow, and therefore less change in pressure within the mouth (Day et al., 2015; Lauder et al., 1986; Muller and Osse, 1984; Sanford and Wainwright, 2002).

Slower times to peak kinematic excursions are expected for larger individuals (Richard and Wainwright, 1995). The size of BassBot (with a jaw length of 11 cm) corresponds to an individual of 55 cm SL according to the scaling relationships of Richard and Wainwright (1995). These predict that a fish of this size should reach peak gape and peak hyoid expansion at 56 and 60 ms, respectively. However, BassBot reached peak gape and hyoid positions four times slower than this in both sets of control trials. This represents a considerable difference between the robotic model and live fish that may be due in part to limitations in the linear motors used to power head expansion. In addition, we note that the biomimetic skin represented relatively high resistive forces during expansion and that this often constrained the speed of our linear motor–tendon units. This indicates that the material properties of the integument surrounding the highly kinetic skull of a suction-feeding fish may play an important role in kinematic behavior of feeding linkages.

Lastly, the large relative size of BassBot may result in a different flow regime within the buccal cavity during expansion relative to smaller live bass. Turbulent flow within the buccal cavity would increase hydrodynamic resistance to buccal expansion and thus reduce subambient pressure generation. For flow within a circular pipe – a reasonable approximation of the buccal space of BassBot – the Reynolds number (*Re*) is calculated as:

$$Re = \frac{VD}{v}, \quad (1)$$

where V, D and v are the flow velocity, pipe diameter and kinematic viscosity of the fluid, respectively. For steady flow within a circular pipe, the transition from laminar to turbulent flow occurs at approximately $2300<Re<4000$ (Cimbala and Cengel, 2008). However, Van Wassenbergh and Aerts (2009) point out that flow within the pipe-like buccal chamber of a suction-feeding centrachid is not steady, but rather rapidly accelerating and decelerating. For flows experiencing even modest accelerations, the transition to turbulent flow occurs around Re=230,000 (Lefebvre and White, 1989). Although we did not measure flow velocities within the robotic buccal cavity, because of the slower kinematic speeds relative to live bass, we presume much slower velocity and acceleration. If the flow regime within the robotic buccal cavity adheres to this simple pipe model, the large size of BassBot would likely increase *Re*. However, we suggest this increase in size is minor when compared with the important effects of accelerating and slower flows within the buccal cavity and, thus, *Re* was unlikely to approach the transition to turbulent flow.

Effect of motor-program speed

The 'slow' treatment had the unexpected effect of increasing peak kinematic displacement and reducing time to peak kinematic displacement for all variables except suspensorial abduction (Table 2, Fig. 6D). Peak excursions of the premaxilla, anterior hyoid and suspensorium were significantly greater in slow trials versus the control (Table 2). The mean time to peak displacement in the slow trials was significantly faster for the gape only and similar to the control. Thus, the overall magnitude of buccal expansion was greater and occurred over a shorter time frame. This resulted in greater magnitudes of subambient pressure and impulse. As discussed above, a faster rate of expansion results in higher velocities and accelerations of flow, and therefore greater subambient pressure within the mouth (Day et al., 2015; Lauder et al., 1986; Sanford and Wainwright, 2002; Svanbäck et al., 2002). The faster acceleration of important linkages resulted from greater magnitudes of force output from our linear motor–tendon units. Like vertebrate muscles, our system's linear motors exhibit a force–velocity trade off. However, the force–velocity relationship of linear motors is convex, whereas the force–velocity relationship of vertebrate muscle is concave; nonetheless, the same principle applies in that slower strain velocities result in greater force output. Therefore, motor programs that imposed slower velocities imparted more force to robotic linkages, and this resulted in faster accelerations and thus greater magnitudes of subambient pressure. This result suggests that suction-feeding fishes may modulate feeding muscle strain velocities to optimize force output and subambient pressure generation. Although scant data exist for operating strain rates during feeding, Carroll and Wainwright (2006) demonstrated that largemouth bass produce high magnitudes of subambient pressure with strain rates below 40% of the maximum shortening velocity.

Effect of restrained hyoid apparatus

In restricting the range of motion of the robotic hyoid apparatus, motion of the hyoid was tightly coupled with movement of the lower jaw (Fig. 7B). This resulted in little suspensorial abduction and no ventral expansion beyond the ventral margin of the lower jaw (Fig. 7B). Without lateral expansion and ventral expansion below the jaw, pressure performance decreased considerably. Peak anterior and posterior subambient pressure was reduced by 47.9% and 51.2%, respectively (Table 2). The duration and magnitude of the subambient pressure change, as indicated by the impulse, was reduced by a similar magnitude of 56.8% and 64.2%, respectively (Table 2). Thus, without the hyoid, and relying solely on the lower jaw for buccal expansion, negative pressure generation is reduced by half. Kinematic behavior of the hyoid apparatus has been implicated

as a major contributor to negative pressure generation (Carroll and Wainwright, 2006; Day et al., 2015). Svanbäck et al. (2002) and Carroll and Wainwright (2006) showed that the motion of the hyoid was a significant factor in multiple regression models of kinematics and pressure. These studies, however, could not identify any causal role played by musculoskeletal units in generating negative pressure. We believe that our experiments with BassBot establish the discrete contribution of hyoid kinematics to suction generation and, furthermore, produce a framework in which to assess the discrete contribution of any other key kinematic parameter to subambient pressure generation. For example, future studies could address the discrete roles of either suspensorial abduction caused by hyoid retraction, ventral rotation of the hyoid apparatus, or both.

The link between reduced suction pressure generation and altered kinematic behavior due to hyoid restriction is clear. Without the lateral and ventral expansion in the posterior region of the buccal cavity that follows expansion in the anterior buccal cavity (Fig. 7A,B,D), water flow dynamics are disrupted by alteration of the anterior-to-posterior expansion gradient. Without the hyoid contribution, the magnitude of posterior buccal expansion is reduced and the timing of posterior expansion is concurrent with anterior expansion (Fig. 7A,B,D). Therefore, water fails to accelerate to the posterior of the buccal chamber, a result indicated by pressure traces with reduced magnitude and earlier peak subambient pressure relative to the control (Fig. 9).

Robotic fabrication, experimentation and future studies

We have demonstrated that a robotic model can faithfully reproduce several key aspects of the kinematic behavior and pressure dynamics of suction-feeding fishes. Using such models, comparative biologists may address open and long-standing questions surrounding the biomechanical basis of feeding in the largest clade of vertebrates. Our two experimental results show that the mechanistic relationships between motor input and musculoskeletal kinematics and flow dynamics can be explored in an entirely new way by precise alterations of model parameters. In the future, modifications of robotic behavior beyond those explored in this study will yield insights into the discrete contribution of other musculoskeletal units and the nature of their interaction with other mechanical systems in the head. For example, future robotic experimentation may focus on whether a trade off exists between hyoid rotation and retraction for suction performance and what biomechanical properties of the teleost feeding system influence the prevalence of either behavior. Also, the role of epaxial musculature in powering suction performance and premaxillary protrusion remains a key area for future work.

Discovery in this realm need not be limited to robotic experiments that focus on kinematic behavior alone. The power of a robotic system in unraveling the biomechanical basis of an organism's behavior also lies in the scientist's ability to alter materials and their properties. For instance, the biomimetic skin of BassBot was a major resistive force to the motor–tendon units. During fabrication and initial testing, before the skin was applied, the kinematic behavior of BassBot was significantly different. Choosing an invariably elastic latex skin imposed the same resistive stress–strain relationship over the entire head. Thus, linkages of low leverage or input forces (e.g. the hyoid bars and suspensorium) are much more restricted in their range of motion than those of high leverage or input forces (e.g. the basihyal, urohyal, basibranchial linkage). Therefore, the choice of skin materials influences the kinematic behavior of linkages in the feeding system and this may reveal where tissue with more viscoelastic properties is required in the fish head.

Lastly, we note that the fabrication of robotic models has great value in understanding the structural relationships within a system as complex as the fish suction-feeding system. By informally assessing how adding or changing important properties of components affects the kinematic behavior, robotic design and fabrication can generate new hypotheses. For example, in our design process, we discovered that the properties of two muscular components were crucial to achieving faithful kinematic behavior. We found that the stiffness of the protractor hyoideus muscle, represented in our model as a rubber band (Fig. 2B), was an important indicator of whether posterior movement of the hyoid resulted in force transmitted laterally to suspensoria through lateral rotation of the hyoid bars or simple ventral rotation of the hyoid apparatus about the interhyal joint. This represents a novel function for the protractor hyoideus, a muscle that is thought to play a primary role in hyoid elevation (Grubich, 2001). Similarly, we discovered that, during expansion, without resistance of the adductor mandibulae linear-motor units, the strain of the axial muscle–tendon unit resulted in lower jaw abduction and little or no lateral expansion. Such an observation may explain why the adductor mandibulae is often active during expansion (Grubich, 2001). These and other observations made during fabrication serve as a rich source of hypotheses that can be tested with robotic models of fish feeding systems.

Acknowledgements

Stacy Farina and Dylan Wainwright read a draft of the manuscript and provided valuable feedback.

Competing interests

The authors declare no competing or financial interests.

Author contributions

C.P.K. and G.V.L. designed the study and robotic model, C.P.K. conducted the experiments, C.P.K. drafted the initial manuscript, C.P.K. and G.V.L. revised the manuscript. C.P.K. fabricated the robotic model and analyzed the data.

Funding

This study was funded with a National Science Foundation Postdoctoral Fellowship in Biology awarded to C.P.K. (award number 1103761).

Supplementary information

Supplementary information available online at
http://jeb.biologists.org/lookup/suppl/doi:10.1242/jeb.132514/-/DC1

References

Aerts, P. (1991). Hyoid morphology and movements relative to abducting forces during feeding in Astatotilapia elegans (Teleostei: Cichlidae). *J. Morphol.* **208**, 323-345.
Alexander, R. (1967). *Functional Design in Fishes*. London: Hutchinson.
Camp, A. L. and Brainerd, E. L. (2014). Role of axial muscles in powering mouth expansion during suction feeding in largemouth bass (*Micropterus salmoides*). *J. Exp. Biol.* **217**, 1333-1345.
Camp, A. L., Roberts, T. J. and Brainerd, E. L. (2015). Swimming muscles power suction feeding in largemouth bass. *Proc. Natl. Acad. Sci. USA* **112**, 8690-8695.
Carroll, A. M. and Wainwright, P. C. (2006). Muscle function and power output during suction feeding in largemouth bass, *Micropterus salmoides*. *Comp. Biochem. Physiol. A Mol. Integr. Physiol.* **143**, 389-399.
Carroll, A. M., Wainwright, P. C., Huskey, S. H., Collar, D. C. and Turingan, R. G. (2004). Morphology predicts suction feeding performance in centrarchid fishes. *J. Exp. Biol.* **207**, 3873-3881.
Cimbala, J. M. and Cengel, Y. (2008). *Essentials of Fluid Mechanics: Fundamentals and Applications*. New York: McGraw-Hill.
Day, S. W., Higham, T. E. and Wainwright, P. C. (2007). Time resolved measurements of the flow generated by suction feeding fish. *Exp. Fluids* **43**, 713-724.
Day, S. W., Higham, T. E., Holzman, R. and Van Wassenbergh, S. (2015). Morphology, kinematics, and dynamics: the mechanics of suction feeding in fishes. *Integr. Comp. Biol.* **55**, 21-35.
De Visser, J. and Barel, C. D. N. (1996). Architectonic constraints on the hyoid's optimal starting position for suction feeding of fish. *J. Morphol.* **228**, 1-18.
Drost, M. R., Muller, M. and Osse, J. W. M. (1988). A quantitative hydrodynamical model of suction feeding in larval fishes: the role of frictional forces. *Proc. R. Soc. Lond. B Biol. Sci.* **234**, 263-281.

Esposito, C. J., Tangorra, J. L., Flammang, B. E. and Lauder, G. V. (2012). A robotic fish caudal fin: effects of stiffness and motor program on locomotor performance. *J. Exp. Biol.* **215**, 56-67.
Ferry-Graham, L. A. and Lauder, G. V. (2001). Aquatic prey capture in ray-finned fishes: a century of progress and new directions. *J. Morphol.* **248**, 99-119.
Grubich, J. R. (2001). Prey capture in actinopterygian fishes: a review of suction feeding motor patterns with new evidence from an elopomorph fish, *Megalops atlanticus*. *Am. Zool.* **41**, 1258-1265.
Grubich, J. R. and Wainwright, P. C. (1997). Motor basis of suction feeding performance in largemouth bass, *Micropterus salmoides*. *J. Exp. Zool.* **277**, 1-13.
Hedrick, T. L. (2008). Software techniques for two- and three-dimensional kinematic measurements of biological and biomimetic systems. *Bioinspir. Biomim.* **3**, 034001.
Higham, T. E., Day, S. W. and Wainwright, P. C. (2006a). Multidimensional analysis of suction feeding performance in fishes: fluid speed, acceleration, strike accuracy and the ingested volume of water. *J. Exp. Biol.* **209**, 2713-2725.
Higham, T. E., Day, S. W. and Wainwright, P. C. (2006b). The pressures of suction feeding: the relation between buccal pressure and induced fluid speed in centrarchid fishes. *J. Exp. Biol.* **209**, 3281-3287.
Holzman, R., Collar, D. C., Mehta, R. S. and Wainwright, P. C. (2012). An integrative modeling approach to elucidate suction-feeding performance. *J. Exp. Biol.* **215**, 1-13.
Lauder, G. V. (1980a). Hydrodynamics of prey capture by teleost fishes. *Biofluid. Mech.* **2**, 161-181.
Lauder, G. V. (1980b). The suction feeding mechanism in sunfishes (*Lepomis*): an experimental analysis. *J. Exp. Biol.* **88**, 49-72.
Lauder, G. V. (1983). Prey capture hydrodynamics in fishes: experimental tests of two models. *J. Exp. Biol.* **104**, 1-13.
Lauder, G. V. (1985). Aquatic feeding in lower vertebrates. In *Functional Vertebrate Morphology* (ed. M. Hildebrand, D. M. Bramble, K. F. Liem and D. B. Wake), pp. 210-229. Cambridge: Harvard University Press.
Lauder, G. V. and Shaffer, H. B. (1985). Functional morphology of the feeding mechanism in aquatic ambystomatid salamanders. *J. Morphol.* **185**, 297-326.
Lauder, G. V., Wainwright, P. C. and Findeis, E. (1986). Physiological mechanisms of aquatic prey capture in sunfishes: functional determinants of buccal pressure changes. *Comp. Biochem. Physiol. A Physiol.* **84**, 729-734.
Lauder, G. V., Anderson, E. J., Tangorra, J. and Madden, P. G. A. (2007). Fish biorobotics: kinematics and hydrodynamics of self-propulsion. *J. Exp. Biol.* **210**, 2767-2780.
Lauder, G. V., Lim, J., Shelton, R. and Witt, C. (2011). Robotic models for studying undulatory locomotion in fishes. *Mar. Tech.* **45**, 41-55.
Lefebvre, P. J. and White, F. M. (1989). Experiments on transition to turbulence in a constant-acceleration pipe flow. *J. Fluids Eng.* **111**, 428-432.
Liem, K. F. (1970). Comparative functional anatomy of the Nandidae (Pisces: Teleostei). *Fieldiana Zool.* **56**, 1-166.
Liem, K. F. (1978). Modulatory multiplicity in the functional repertoire of the feeding mechanism in cichlid fishes. I. Piscivores. *J. Morphol.* **158**, 323-360.
Meijering, E., Dzyubachyk, O. and Smal, I. (2012). Methods for cell and particle tracking. *Methods Enzymol.* **504**, 183-200.
Motta, P. J. and Wilga, C. D. (2000). Advances in the study of feeding behaviors, mechanisms, and mechanics of sharks. *Environ. Biol. Fish.* **20**, 1-26.
Muller, M. and Osse, J. W. M. (1984). Hydrodynamics of suction feeding in fish. *Trans. Zool. Soc. Lond.* **37**, 51-135.
Nauwelaerts, S., Wilga, C. D., Lauder, G. V. and Sanford, C. P. (2008). Fluid dynamics of feeding behaviour in white-spotted bamboo sharks. *J. Exp. Biol.* **211**, 3095-3102.
Nyberg, D. W. (1971). Prey capture in the largemouth bass. *Am. Midl. Nat.* **86**, 128-144.
Osse, J. W. and Muller, M. (1980). A model of suction feeding in teleostean fishes with some implications for ventilation. In *Environmental Physiology of Fishes* (ed. M. A. Ali), pp. 335-352. New York: Plenum.
Richard, B. and Wainwright, P. (1995). Scaling the feeding mechanism of largemouth bass (*Micropterus salmoides*): kinematics of prey capture. *J. Exp. Biol.* **198**, 419-433.
Sanford, C. P. J. and Wainwright, P. C. (2002). Use of sonomicrometry demonstrates the link between prey capture kinematics and suction pressure in largemouth bass. *J. Exp. Biol.* **205**, 3445-3457.
Svanbäck, R., Wainwright, P. C. and Ferry-Graham, L. A. (2002). Linking cranial kinematics, buccal pressure, and suction feeding performance in largemouth bass. *Physiol. Biochem. Zool.* **75**, 532-543.
Van Wassenbergh, S. and Aerts, P. (2009). Aquatic suction feeding dynamics: insights from computational modelling. *J. R. Soc. Interface* **6**, 149-158.
Wainwright, P. and Richard, B. (1995). Scaling the feeding mechanism of the largemouth bass (*Micropterus salmoides*): motor pattern. *J. Exp. Biol.* **198**, 1161-1171.
Wainwright, P., Carroll, A. M., Collar, D. C., Day, S. W., Higham, T. E. and Holzman, R. A. (2007). Suction feeding mechanics, performance, and diversity in fishes. *Integr. Comp. Biol.* **47**, 96-106.
Westneat, M. W. (2004). Evolution of levers and linkages in the feeding mechanisms of fishes. *Integr. Comp. Biol.* **44**, 378-389.
Westneat, M. W. (2005). Skull biomechanics and suction feeding in fishes. In *Fish Biomechanics* (ed. R. E. Shadwick and G. V. Lauder), pp. 29-75. San Diego: Elsevier.
Wilga, C. D. and Sanford, C. P. (2008). Suction generation in white-spotted bamboo sharks *Chiloscyllium plagiosum*. *J. Exp. Biol.* **211**, 3128-3138.